

---

# ENERGY-BASED PINNs FOR SOLVING COUPLED FIELD PROBLEMS: CONCEPTS AND APPLICATION TO THE OPTIMAL DESIGN OF AN INDUCTION HEATER

---

A PREPRINT

 **Marco Baldan**

Department of Optimization  
Fraunhofer ITWM  
Kaiserslautern, Germany  
marco.baldan@itwm.fraunhofer.de

 **Paolo Di Barba**

Department of Electrical, Computer & Biomedical Engineering  
University of Pavia  
Pavia, Italy  
paolo.dibarba@unipv.it

February 12, 2024

## ABSTRACT

Physics-informed neural networks (PINNs) are neural networks (NNs) that directly encode model equations, like Partial Differential Equations (PDEs), in the network itself. While most of the PINN algorithms in the literature minimize the local residual of the governing equations, there are energy-based approaches that take a different path by minimizing the variational energy of the model. We show that in the case of the steady thermal equation weakly coupled to magnetic equation, the energy-based approach displays multiple advantages compared to the standard residual-based PINN: it is more computationally efficient, it requires a lower order of derivatives to compute, and it involves less hyperparameters. The analyzed benchmark problem is the optimal design of an inductor for the controlled heating of a graphite plate. The optimized device is designed involving a multi-physics problem: a time-harmonic magnetic problem and a steady thermal problem. For the former, a deep neural network solving the direct problem is supervisedly trained on Finite Element Analysis (FEA) data. In turn, the solution of the latter relies on a hypernetwork that takes as input the inductor geometry parameters and outputs the model weights of an energy-based PINN (or ePINN). Eventually, the ePINN predicts the temperature field within the graphite plate.

**Keywords** Physics-informed neural network · Variational formulation · Optimal design · Coupled problem · Inverse problem

## 1 Introduction

Physics-Informed Neural Networks are neural networks that encode model equations, like PDEs, as a component of the neural network itself [1]. PINNs are nowadays used to solve PDEs, stochastic PDEs, fractional, and integral-differential equations in a wide range of applications in both science and engineering. For the most part of the available literature, PINNs are trained by minimizing a neural network loss function that includes terms reflecting the initial (ICs) and boundary conditions (BCs) along the space-time domain's boundary and the PDE residual at selected points in the domain (called collocation points) [2]. However, some researchers adopt the variational form of PDEs and minimize the corresponding energy functional [3]. This approach has been successfully adopted in, e.g., computational mechanics [4], [5], [6], and it could be applied in case the governing PDEs can be derived from a known functional. This is the case, among others, for the Laplace, Poisson and Helmholtz equations [7].

Induction heating is generally used for thermal processes of materials [8]. In fact it allows a good temperature control of the work-piece temperature with a high efficiency. In this field, the solution of weakly coupled (quasi-static) magnetic and thermal problems is mandatory [9]. The magnetic problem is typically solved in the frequency domain, while, depending on the application, the thermal solution is either time transient or steady-state. In the present work, we will

focus on the steady case. There is little literature available involving PINNs for solving quasi-static time-harmonic magnetic problems [10]. On the contrary, albeit not involving induction heating applications, PINNs have been often adopted for the solution of time transient [11], [12] and steady [13], [14] heat conduction problems. However, in the existing literature, PINN's training for the steady heat problem relies on the minimization of the PDE residual [13], [14]. In this work, on the one hand, we will show the benefits of adopting the energy-based approach compared to the strong residual method. First, it is more computationally efficient, i.e., with the same network architecture and the same amount of collocation points, less training epochs are required to achieve a prescribed accuracy in the temperature field. Second, it involves a lower order of derivatives (first rather than second), therefore allowing material discontinuities in the domain. The first and second advantages imply a significant speed up in network training. Finally, it requires less (or no) hyperparameters in the loss, making the training more robust. On the other hand, we want to assess new approaches in the induction heating framework. The current work differs from already existing contributions [10], [15], [16], [17]. In [10], authors introduce PINNs in a magnetic-thermal coupled problem, but still relying on the conventional residual-based approach and considering a toy one-dimensional example. In [15], a convolutional neural network (CNN) is trained on FEA generated temperature maps to solve an identification problem. [16] deals with an orthogonal decomposition method to build a data-driven digital twin. Finally, in [17] it is investigated the explainability of black-box models trained on real-world data concerning surface hardening. In this work, the analyzed benchmark problem is the design of an inductor for the controlled heating of a graphite plate (adapted from [18]). A first neural network (called mNN) approximates the time-harmonic magnetic solution and it maps the design variables (or system parameters, in the current benchmark it is the inductor geometry) to the Joule loss distribution. mNN is supervisely trained on FEA simulations. Second, an energy-based PINN is trained (tePINN) to solve the temperature field for a particular set of system parameters. Finally, a hypernetwork [19] (called tHNN), which takes as input the design variables and outputs the model weights of a tePINN [20], is used. In turn, the tePINN predicts the temperature field within the graphite plate. It is worth underlying that both tePINN and tHNN do not rely on any (e.g., FEA) data. Moreover, in order to train the tHNN, mNN is needed to provide the joule loss distribution, that is the source term in the heat equation. It follows that, once trained, the tHNN provides the fast (i.e., it only requires two forward passes) solution of a parametric coupled problem. By combining the tHNN with an optimizer, it gives the opportunity of quickly solving an inverse (e.g., optimal design) problem.

The paper is structured as follows: section 2 introduces the energy-based physics-informed neural network framework. Section 3 describes the benchmark problem and the use of neural networks to solve the design problem. Finally, section 4 concludes the paper.

## 2 Energy-based Physics-Informed Neural Networks

Consider, without loss of generality, the 2D boundary value problem:

$$-\frac{\partial}{\partial x} \left( \alpha_x \frac{\partial \phi}{\partial x} \right) - \frac{\partial}{\partial y} \left( \alpha_y \frac{\partial \phi}{\partial y} \right) + \beta \phi = f \text{ in } \Omega \quad (1)$$

where  $\phi$  is the unknown function,  $\alpha_x$ ,  $\alpha_y$ , and  $\beta$  are known parameters, which could be position-dependent functions, associated with the physical properties of the domain, and  $f$  is the source or excitation function [7]. We assume that  $\alpha_x$ ,  $\alpha_y$  are continuous over the entire domain. The boundary conditions to be considered are:

$$\phi = p \text{ on } \Gamma_1 \quad (2)$$

and

$$\left( \alpha_x \frac{\partial \phi}{\partial x} \vec{x} + \alpha_y \frac{\partial \phi}{\partial y} \vec{y} \right) \cdot \vec{n} + \gamma \phi = q \text{ on } \Gamma_2 \quad (3)$$

where  $\Gamma = \Gamma_1 + \Gamma_2$  denotes the contour enclosing the area,  $\vec{n}$  is the normal unit vector,  $\gamma$ ,  $p$  and  $q$  are known parameters associated with physical properties on the boundary. The variational problem equivalent to the boundary-value problem is given by [7]:

$$\begin{cases} \delta F(\phi) = 0 \\ \phi = p \text{ on } \Gamma_1 \end{cases} \quad (4)$$

with functional  $F$  defined as:

$$F(\phi) = \frac{1}{2} \iint_{\Omega} \left[ \alpha_x \left( \frac{\partial \phi}{\partial x} \right)^2 + \alpha_y \left( \frac{\partial \phi}{\partial y} \right)^2 + \beta \phi^2 \right] d\Omega + \int_{\Gamma_2} \left( \frac{\gamma}{2} \phi^2 - q\phi \right) d\Gamma - \iint_{\Omega} f\phi d\Omega. \quad (5)$$

It is assumed all parameters and functions to be real-valued, therefore this functional is real-valued too. It can be shown that Eq. 4 has a unique solution, i.e., the functional has a unique minimum. In case of the 2D steady heat conduction equation,  $\phi$  corresponds to the temperature  $T$ ,  $f$  denotes the heat source density  $Q$ . In a weakly coupled electro-thermal problem the source term  $Q$  takes induced current loss into account (more details in section 3.2). Considering an anisotropic material  $\alpha_x = \alpha_y = \lambda$  ( $\lambda$  is the heat conductivity) subject to Dirichlet and Robin BCs ( $p = T_{ref}$  is a specified temperature, having  $\gamma = h$ , where  $h$  is the overall heat transfer coefficient,  $q = hT_0$ ,  $T_0$  being the external temperature), the system of governing equations becomes:

$$-\frac{\partial}{\partial x} \left( \lambda \frac{\partial T}{\partial x} \right) - \frac{\partial}{\partial y} \left( \lambda \frac{\partial T}{\partial y} \right) = Q \text{ in } \Omega \quad (6)$$

with

$$T = T_{ref} \text{ in } \Gamma_1 \quad (7)$$

and

$$\left( \lambda \frac{\partial T}{\partial x} \vec{x} + \lambda \frac{\partial T}{\partial y} \vec{y} \right) \cdot \vec{n} + hT = hT_0 \text{ on } \Gamma_2 \quad (8)$$

with the functional:

$$F(T) = \frac{1}{2} \iint_{\Omega} \left[ \lambda \left( \frac{\partial T}{\partial x} \right)^2 + \lambda \left( \frac{\partial T}{\partial y} \right)^2 \right] d\Omega + \int_{\Gamma_2} \left( \frac{h}{2} T^2 - hT_0 T \right) d\Gamma - \iint_{\Omega} QT d\Omega. \quad (9)$$

Introducing now the energy-based PINN  $\mathcal{N}_p$  (tePINN) with weights (including biases)  $\theta_p$ , its loss function to minimize corresponds to the functional:

$$L_p(\theta_p) = \frac{1}{2} \iint_{\Omega} \left[ \lambda \left( \frac{\partial \hat{T}(\mathbf{x}, \theta_p)}{\partial x} \right)^2 + \lambda \left( \frac{\partial \hat{T}(\mathbf{x}, \theta_p)}{\partial y} \right)^2 \right] d\Omega + \int_{\Gamma_2} \left( \frac{h}{2} \hat{T}^2(\mathbf{x}, \theta_p) - hT_0 \hat{T}(\mathbf{x}, \theta_p) \right) d\Gamma + \quad (10)$$

$$- \iint_{\Omega} Q \hat{T}(\mathbf{x}, \theta_p) d\Omega$$

Derivatives are obtained via automatic differentiation (AD). The predicted temperature field is  $\hat{T}(\mathbf{x}; \theta_p) = a + b\mathcal{N}_p(\mathbf{x}; \theta_p)$ , with  $a$  and  $b$  user-defined scalar values. Either trapezoidal rule or Monte Carlo integration can be used for computing the integral by sampling the domain with either randomly or uniformly spaced points. However, with this approach, a large number of integration points are usually required to obtain accurate results. To address this issue, we prefer the Gauss quadrature rule, with a sampling strategy that is close to a meshing step in conventional FEA (a weakness in this case of the energy-based approach, especially in case of complex geometries):

$$L_p^E(\theta_p) = \frac{1}{2} \sum_{i=1}^{N_{\Omega}} A_i \sum_{k=1}^{N_G} \lambda_{i,k} \left[ \left( \frac{\partial \hat{T}(\mathbf{x}_{i,k}, \theta_p)}{\partial x} \right)^2 + \left( \frac{\partial \hat{T}(\mathbf{x}_{i,k}, \theta_p)}{\partial y} \right)^2 \right] \quad (11)$$

$$+ \sum_{i=1}^{N_{\Gamma_2}} l_i \sum_{k=1}^{N_g} \left( \frac{h}{2} \hat{T}^2(\mathbf{x}_{i,k}, \theta_p) - hT_0 \hat{T}(\mathbf{x}_{i,k}, \theta_p) \right) - \sum_{i=1}^{N_{\Omega}} A_i \sum_{k=1}^{N_G} Q_{i,k} \hat{T}(\mathbf{x}_{i,k}, \theta_p)$$

where  $N_{\Omega}$  and  $N_{\Gamma_2}$  is the number of discretization elements of the domain and the  $\Gamma_2$  boundary, respectively.  $N_G$  denotes the number of integration points for each element,  $A$  and  $l$  are area and length of the corresponding element, respectively. The discretization (i.e., sampling points) remains unchanged while training. For the sake of completeness, we mention that the residual-based PINN loss would be:

$$\begin{aligned}
L_p^R(\boldsymbol{\theta}_p) = & \frac{1}{S_\Omega} \sum_{j=1}^{S_\Omega} \left[ -\frac{\partial}{\partial x} \left( \lambda_j \frac{\partial \hat{T}(\mathbf{x}_j, \boldsymbol{\theta}_p)}{\partial x} \right) + -\frac{\partial}{\partial y} \left( \lambda_j \frac{\partial \hat{T}(\mathbf{x}_j, \boldsymbol{\theta}_p)}{\partial y} \right) - Q_j \right]^2 + \frac{\eta_1}{S_{\Gamma_1}} \sum_{j=1}^{S_{\Gamma_1}} \left[ \hat{T}(\mathbf{x}_j, \boldsymbol{\theta}_p) - T_{ref} \right]^2 \\
& + \frac{\eta_2}{S_{\Gamma_2}} \sum_{j=1}^{S_{\Gamma_2}} \left[ \lambda_j \frac{\partial \hat{T}(\mathbf{x}_j, \boldsymbol{\theta}_p)}{\partial n} + h \hat{T}(\mathbf{x}_j, \boldsymbol{\theta}_p) - h T_0 \right]^2
\end{aligned} \tag{12}$$

with  $S_\Omega$ ,  $S_{\Gamma_1}$ ,  $S_{\Gamma_2}$  the amount of collocation points within the domain, on the  $\Gamma_1$  and  $\Gamma_2$  boundaries, respectively. It stands out that the residual-based loss involves second derivatives (instead first derivatives only appear in Eq. 11) and needs hyperparameters ( $\eta_1$ ,  $\eta_2$  - no one appears in the energy-based loss). The presented physics-informed neural network does not take any system parameter (like geometry or material properties) as input, therefore, when embedded in inverse problems, solving the PDE governing equations, it would require additional training for each new system parameter set. In this sense, transfer learning (TL) would help [23]. However, we prefer a hypernetwork (tHNN - "thermal" HNN)  $\mathcal{N}_h$  [19] (whose weights are  $\boldsymbol{\theta}_h$ ) that receives system parameters ( $\boldsymbol{\xi}$ ) and outputs the network weights of the tePINN ("thermal" ePINN), which in turn provides the solution of the direct thermal problem [20], [21]. In fact, tePINN predicts the temperature evaluated at  $\mathbf{x}$ . The tHNN loss function is:

$$L_h(\boldsymbol{\theta}_h) = \sum_{i=1}^{N_\xi} L_p^E(\mathcal{N}_h(\boldsymbol{\xi}^i; \boldsymbol{\theta}_h)) \tag{13}$$

$N_\xi$  indicates the number of system parameter sets involved in a batch. More about the training in section 3.2. Once trained, the hypernetwork is able to predict the temperature map for a given system parameter set. Therefore, solving the inverse problems with  $\boldsymbol{\xi}$  as design variables is associated with a little computational cost. Moreover, it is straightforward to consider different and/or multiple objectives. Finally, the optimizer can take advantage of known derivatives (objective w.r.t. design parameters) due to AD [21]. More details in section 3.2.

### 3 The benchmark problem

The 2D benchmark (adapted from [18] - planar unlike axisymmetric geometry (this represents no limitation regarding the applications of the presented approach)) includes a graphite (electrical and thermal properties at 1200°C:  $\rho_g = 7.76 \cdot 10^{-6} \Omega\text{m}$ ,  $\mu_{r,g} = 1$ ,  $\lambda = 60 \text{ W/(mK)}$ ) plate of width 240 mm and thickness 14 mm (for symmetry reasons only half of it is considered) and a 8-turn induction heater (made of copper,  $\rho_c = 2 \cdot 10^{-8} \Omega\text{m}$ ,  $\mu_{r,c} = 1$ ) (Fig. 1). All turns, series connected, carry a current of 400 Arms at 4250 Hz. The plate is supposed to achieve a steady-state average temperature around 1100-1150°C, as required by the industrial process. Due to the desired temperature uniformity, material parameters are not temperature dependent [18].

#### 3.1 Field model: a coupled magnetic-thermal analysis

The direct problem involves a time-harmonic quasi-static magnetic problem (to evaluate the power density in the graphite plate) coupled to a steady-state thermal problem (to evaluate the temperature profile). The magnetic problem is formulated in terms of the phasor of the magnetic vector potential  $\dot{\mathbf{A}}$ :

$$\nabla^2 \dot{\mathbf{A}} - j\omega\mu\rho^{-1}\dot{\mathbf{A}} = -\mu\dot{\mathbf{J}} \tag{14}$$

where  $\dot{\mathbf{J}}$  is the phasors of the current density,  $\mu$  is the magnetic permeability,  $\rho$  is the electrical resistivity and  $\omega$  is the magnetic field pulsation. The solutions of the magnetic and thermal problem are weakly coupled by means of the source term:

$$f = \rho^{-1}\omega^2|\dot{\mathbf{A}}|^2 \tag{15}$$

of the thermal equation (Eqs. 6–8). The thermal domain is the graphite plate. Along the axis of symmetry (i.e., at  $x=0$ ), Neumann BCs are imposed. At the other bounds, Robin BCs are adopted with overall heat exchange coefficient of 50 W/(m<sup>2</sup>K) and external temperature of 50°C (Fig. 1). The overall heat exchange coefficient is meant to already include the radiation losses.

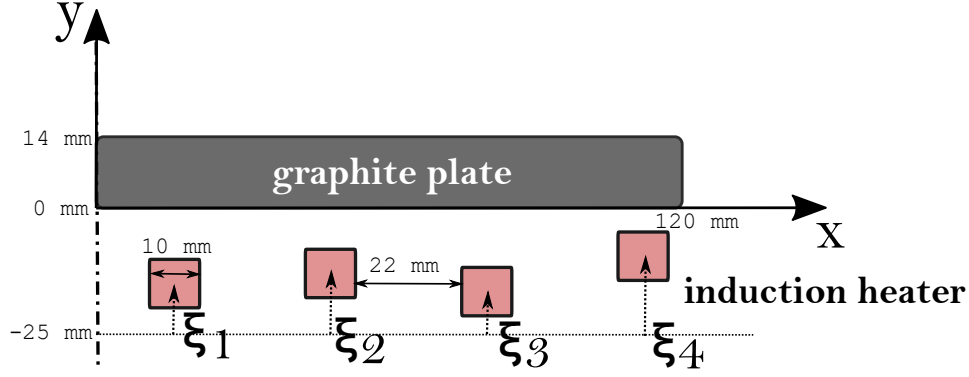


Figure 1: Benchmark setup (half of it due to symmetry).

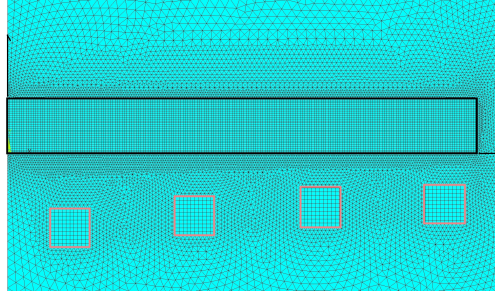


Figure 2: Particular of the mesh (graphite plate and induction heater) used in the FEA.

## 3.2 Approximating and solving the direct problem

### 3.2.1 Magnetic analysis

A fully-connected neural network (mNN - "magnetic" NN) with 3 hidden layers of 128 neurons each is supervisedly trained to map the inductor geometry (i.e., the y-position of each turn -  $\xi = [\xi_1, \xi_2, \xi_3, \xi_4]$  - Fig. 1) and the space position (x, y) with the heat source density ( $f$ ) (Eq. 15) within the graphite plate. FEA simulations run at different system parameter sets, with a uniform discretization (range 5 to 15 mm) covering 6 values for each variable and a total of 1296 magnetic solutions, constitutes the training data-set. Since the elements of the mesh in the FEA (Fig. 2) do not coincide with those adopted for tePINN's or tHNN's (Eq. 11) training, each FEA solution is projected to the Gauss integration points adopting a piecewise cubic, continuously differentiable, and approximately curvature-minimizing polynomial approximation (see `scipy.interpolate.griddata` [22]). Interpolated data actually serves as training data-set for the mNN. 30 additional random inductor geometries and their corresponding FEA simulations form the test-data set, instead. FEA is performed with a commercial software [24]. The model has  $5 \cdot 10^4$  linear elements (Fig. 2).

The activation function of mNN is  $\max(0; x^3)$ . It is trained on  $4 \cdot 10^4$  epochs using the ADAM optimizer. The mean absolute error (MAE) on the test-set (evaluated at  $10^4$  positions of each of the 30 random inductor geometries) is equal to  $2.05 \cdot 10^3 \text{ W/m}^3$ , which means 0.08% in percentage terms. The maximum absolute error is instead  $5.45 \cdot 10^3 \text{ W/m}^3$  (2.2%). See an exemplary case in Fig. 3.

### 3.2.2 Single thermal analysis - tePINN

The architecture of tePINN is a fully-connected neural network with 2 hidden layers with 64 neurons each. We consider a specific inductor geometry ( $\xi_1 = 14.8 \text{ mm}$ ,  $\xi_2 = \xi_3 = \xi_4 = 15 \text{ mm}$ ) and use, only here, the FEA solution for the distribution of the heat source density (in particular, a cubic interpolation to the collocation and integration points - see `scipy.interpolate.griddata` [22]). In the thermal domain (i.e., the graphite plate),  $10^4$  elements (all equal) are considered. Integration relies on the 2-point Gaussian quadrature. For sake of comparison, a residual-driven PINN, having the same architecture, adopting the same amount of collocation points, and taking the same weight initialization, is trained as

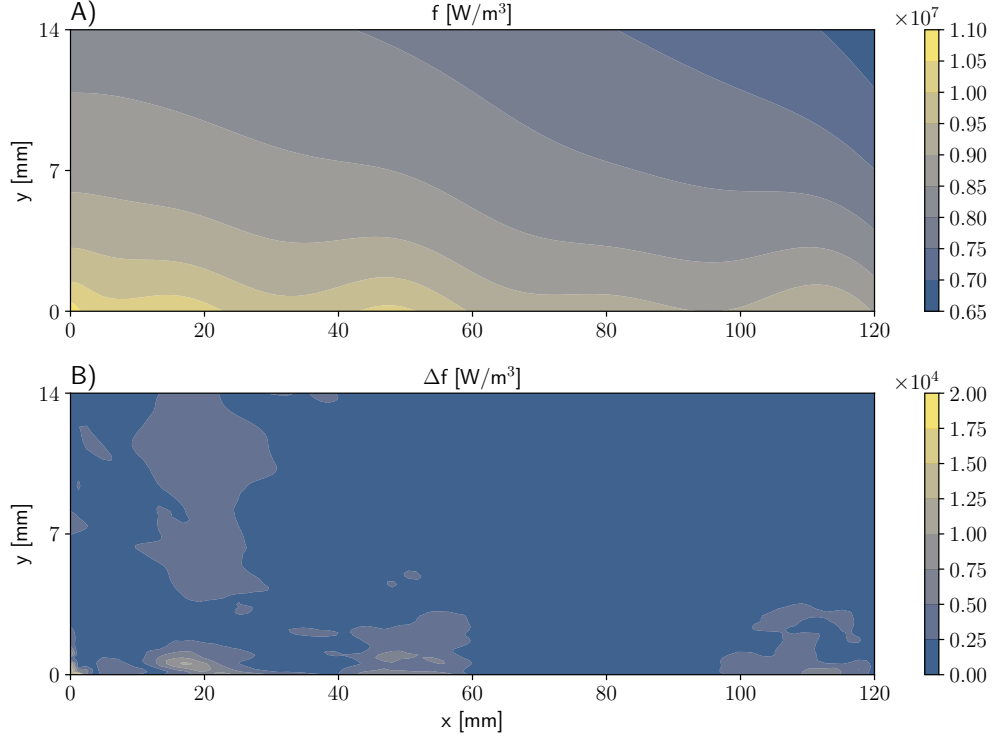


Figure 3: Estimating the accuracy of the mHH for a random test inductor geometry ( $\xi_1 = 13.63$  mm,  $\xi_2 = 13.59$  mm,  $\xi_3 = 9.59$  mm,  $\xi_4 = 12.67$  mm). A) Joule losses within the graphite plate. B) Absolute error taking the FEA solution as ground truth.

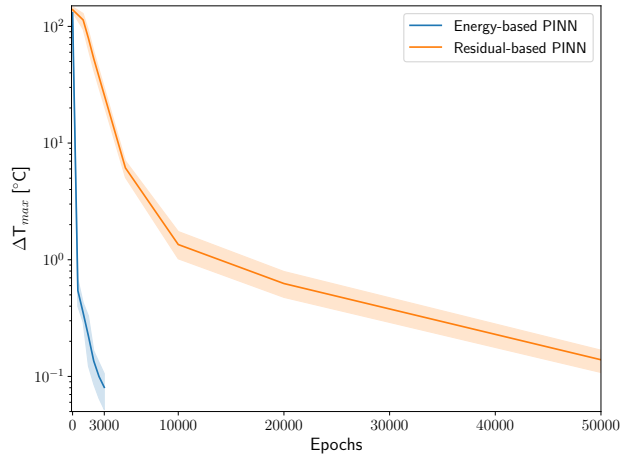


Figure 4: Max absolute error in the temperature field solution (ground truth is the FEA solution). The residual-based PINN takes  $\eta_2 = 10^3$  in the loss function.

well. Considering the FEA solution as the ground truth, the maximum absolute error behaves in the two approaches much differently (Fig. 4).

The energy-based approach shows a much faster learning and it is characterized by a solution error around  $0.1^\circ\text{C}$  after just  $3 \cdot 10^3$  epochs. On the contrary, the residual-based approach takes approximately  $5 \cdot 10^4$  epochs to achieve a comparable accuracy. Looking at the computation time on a personal laptop, the advantage of adopting the energy-based PINN is even larger (here approximately a factor 50), due to the lower order of derivatives involved. Since the residual-based

loss (Eq. 12) involves hyperparameters (in this benchmark only  $\eta_2$ , since no Dirichlet BCs are imposed), obtained results concern the best achieved among  $\eta_2 = [10^1, 10^2, 10^3, 10^4, 10^5]$ , namely with  $\eta_2 = 10^3$ .

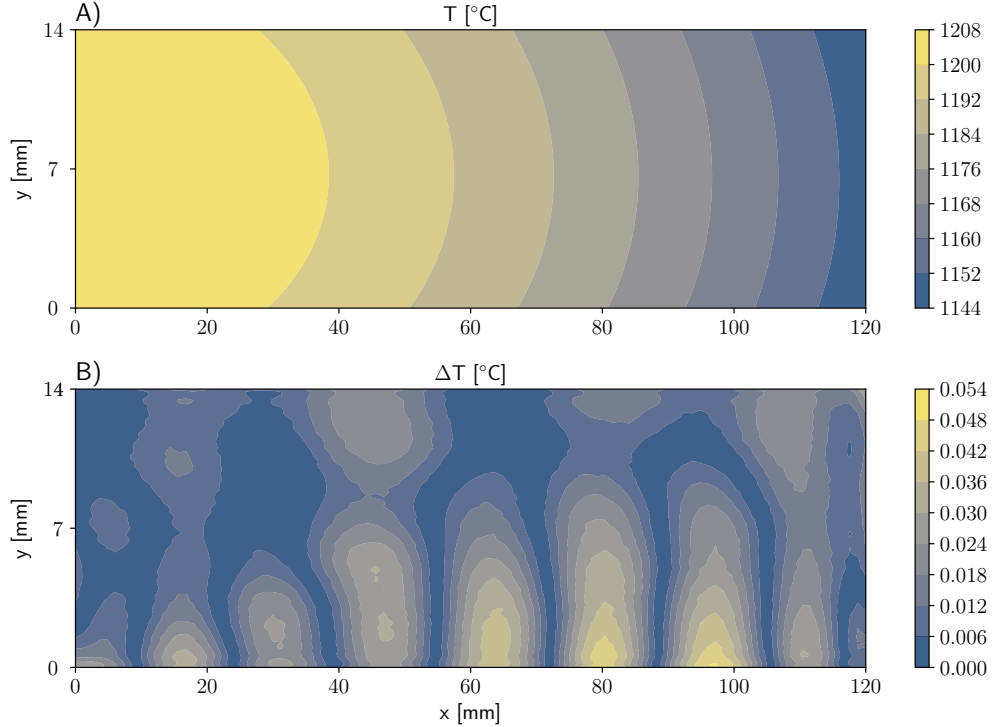


Figure 5: Estimating accuracy of the tePINN prediction in case of a given inductor geometry ( $\xi_1 = 14.8$  mm,  $\xi_2 = \xi_3 = \xi_4 = 15$  mm). The heat source distribution comes from FEA solution. A) Temperature field within the graphite plate. B) Absolute error taking the FEA solution as ground truth.

### 3.2.3 Parametric thermal analysis - tHNN

Also tHNN is a fully-connected neural network. It has 4 inputs and it outputs the weights and biases of a tePINN, now only having 2 hidden layers with 24 neurons each (compared to previous section, less tePINN weights are preferred to limit the output dimension of tHNN). tHNN has also 2 hidden layers, but the number of neurons is 128. ReLU is the chosen activation function. The tHNN is trained on  $10^3$  epochs (the batch size  $N_{\xi}$  is 8 - Eq. 13) with ADAM. Since this involves the solution of a coupled problem, the mHH is required, in the training framework, to predict the heat source map  $Q$  (Fig. 6).

The temperature field provided by the trained tHNN is tested in case of 30 random inductor geometries. The MAE is  $0.15^{\circ}\text{C}$ , while the maximum absolute error is  $0.47^{\circ}\text{C}$ . This is almost a factor five higher than the single thermal analysis of previous section, but still represents an error lower than 0.5% in relative terms. In fact, we are now dealing with a coupled problem in which both the magnetic and thermal solutions are approximated (in 3.2.2, the ground truth heat source distribution is considered, instead).

### 3.3 The inverse problem: inductor design for uniform heating

Once tHNN is trained, it is able to predict the entire temperature field for a given induction geometry. It takes two forward passes: in the first, the tHNN delivers the network weights of the corresponding tePINN, in the second, the tePINN predicts the temperature at locations  $X$ . It means that an inverse problem is generally fast to be solved. Moreover, due to AD, the optimizer could take advantage of the derivatives (Fig. 7). We note that the objective function of the inverse problem is defined a-posteriori without posing any restriction to the training of the tHNN.

In the following benchmark, the objective measures, using the "criterion of proximity", the temperature in-homogeneity. It is evaluated at the plate's upper boundary [18]:

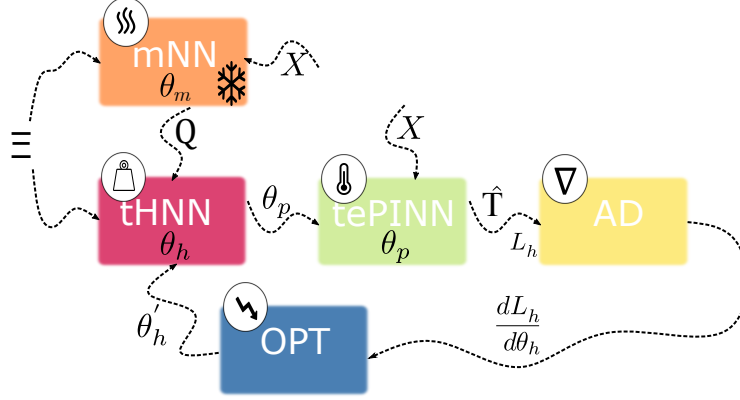


Figure 6: Training scheme of tHNN involving a coupled magnetic-thermal problem. mNN has been previously trained (it has now frozen weights) and it outputs the heat source density at a given design parameter set  $\xi$  evaluated at position  $X$ . tePINN receives the weights from tHNN and it predicts the temperature at location  $X$ . The objective to be minimized is  $L_h$  (Eq. 13).

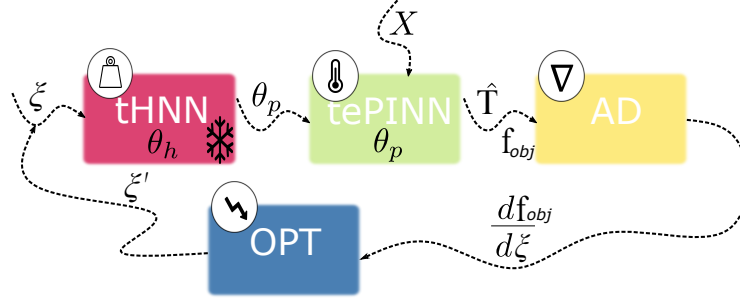


Figure 7: Solving the inverse problem involving tHNN. tHNN has now frozen weights. tePINN receives the weights from tHNN and it predicts the temperature at location  $X$ . The objective to minimize is  $f_{obj}$  and it comes from the design problem (Eq. 16).

$$f_{obj}(\xi) = 1 - \frac{N_j(|T_j(\xi) - T_{goal}| < \text{tol})}{N_{max}} \quad (16)$$

where  $N_{max}$  is the number of sampling points (200),  $T_{goal} = 1130^\circ\text{C}$  is the temperature which should be reached in the plate, and  $\text{tol} = 10^\circ\text{C}$  (approx. 1% in relative terms). We adopt a differential evolution as optimizer [22] and solve two inverse problems: the first, involving tHNN for the parametric solution of the coupled problem (mNN is now no longer needed), the second using FEA instead. Both problems achieve the same optimal objective of 0.02, meaning that actually almost the entire upper graphite plate bound lies within the prescribed temperature tolerance (Fig. 8). Looking at the design variables, the discrepancy never overcomes 0.1 mm (Tab. 1). Solving the inverse problem requires approximately 20 seconds on a CPU of a personal laptop. When adopting FEA for the field analysis instead, the computational time for the solution of the inverse problem rises at  $10^4$  seconds. Parallelizing the calculations and/or adopting a GPU would certainly significantly reduce the computation time. However, this is beyond the scope of this work.

## 4 Conclusion

In this paper, we introduce the use of energy-based PINNs for solving the steady-state heat conduction equation. Compared to the residual-based approach, it shows multiple advantages, including a drastic reduction of the training time (even a factor 50 in the considered benchmark) and no use of hyperparameters in the loss function. On the contrary, it requires performing integration that, with the Gauss quadrature method, needs a sampling strategy close to a meshing step in conventional FEA. The parametric solution of the magnetic-thermal coupled problem makes use



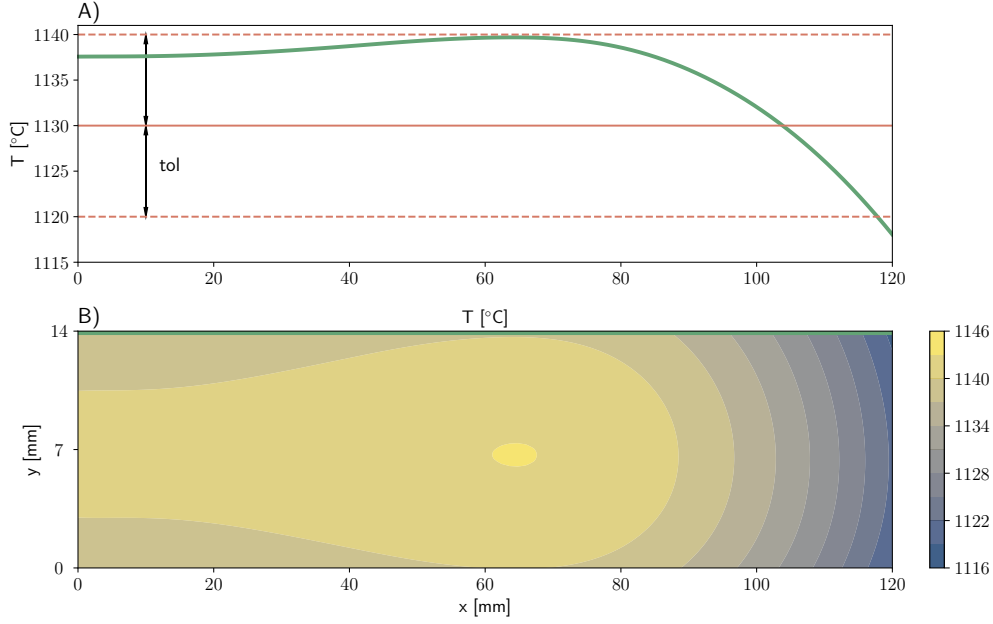


Figure 8: Results of the inductor optimal design. A) Optimized temperature profile of the graphite plate upper bound. B) Optimized temperature field.

Table 1: Design variable and their ranges

Design variable	$l_b$	$u_b$	Start	Opt FEA	Opt tHNN
$\xi_1$	5	15	14.8	5.1	5.1
$\xi_2$	5	15	15	5.3	5.4
$\xi_3$	5	15	15	11.0	10.9
$\xi_4$	5	15	15	14.9	14.9

of FEA simulations to approximate the magnetic solution, while the thermal analysis results entirely unsupervised (due to the hypernetwork). The proposed framework achieves an accuracy that allows to solve an optimal inductor design problem (therefore involving a multi-physics analysis) with an objective that is defined a-posteriori (i.e., after the hypernetwork’s training). Such a framework could be adopted, e.g., in the fast prototyping of inductors, due to both the freedom in defining the design objective(s) and little computational cost. Moreover, a multi-criteria design would be straightforward. The obtained results are promising and motivate continuation of the researches and extension of them to the design of, e.g., various industrial electromagnetic devices.

## References

- [1] S. Cuomo, V.S. Di Cola, F. Giampaolo, G. Rozza, M. Raissi and F. Piccialli. Scientific Machine Learning through Physics-Informed Neural Networks: Where we are and what’s next. In *J. Sci. Comput.*, 92, 2022.
- [2] M. Raissi, P. Perdikaris, G.E. Karniadakis. Physics-informed neural networks: A deep learning framework for solving forward and inverse problems involving nonlinear partial differential equations. In *J. Comp. Physics*, pp. 686-707, 378, 2019.
- [3] W. E and B. Yu. The Deep Ritz Method: A Deep Learning-Based Numerical Algorithm for Solving Variational Problems, In *Commun. Math. Stat.*, pp. 1-12, 6, 2018.
- [4] E. Samaniego, C. Anitescu, S. Goswami, V.M. Nguyen-Thanh, H. Guo, K. Hamdia, X. Zhuang, T. Rabczuk. An energy approach to the solution of partial differential equations in computational mechanics via machine learning: Concepts, implementation and applications. In *Comput. Methods Appl. Mech. Engrg.*, 112790, 362, 2020.
- [5] S. Goswami, C. Anitescu, S. Chakraborty, T. Rabczuk. Transfer learning enhanced physics informed neural network for phase-field modeling of fracture. In *Theoretical and Applied Fracture Mechanics*, 102447, 106, 2020.

- [6] W. Li, M. Bazant, J. Zhu. A physics-guided neural network framework for elastic plates: Comparison of governing equations-based and energy-based approaches. In *Comput. Methods Appl. Mech. Engr.*, 113933, 383, 2021.
- [7] J.M. Jin. *The Finite Element Method in Electromagnetics*. Wiley, 2014.
- [8] S. Lupi, M. Forzan, A. Aliferov. *Induction and Direct Resistance Heating*. Springer International, 2015.
- [9] A. Candeo, C. Ducassy, P. Bocher and F. Dughiero. Multiphysics modeling of induction hardening of ring gears for the aerospace industry. In *IEEE Transactions on Magnetics*, pp. 918-921, 47(5), 2011.
- [10] M. Baldan, G. Baldan and B. Nacke. Solving 1D nonlinear magneto quasistatic Maxwell's equations using neural networks. In *IET Science, Measurement and Technology*, pp. 204-217, 15(2), 2021.
- [11] M.S. Go, J.M. Lim and S. Lee. Physics-informed neural network-based surrogate model for a virtual thermal sensor with real-time simulation. In *Int. J. of Heat and Mass Transfer*, 124392, 214, 2023.
- [12] F. Bragone, K. Morozovska, P. Hilber, T. Laneryd, M. Luvisotto. Physics-informed neural networks for modelling power transformers dynamic thermal behaviour. In *Electric power systems research*, 108447, 211, 2022.
- [13] Z. Xing, H. Cheng and J. Cheng. Deep Learning Method Based on Physics-Informed Neural Network for 3D Anisotropic Steady-State Heat Conduction Problems. In *Mathematics*, 4049, 11, 2023.
- [14] S. Koric, D.W. Abueidda. Data-driven and physics-informed deep learning operators for solution of heat conduction equation with parametric heat source. In *Int. J. of Heat and Mass Transfer*, 123809, 203, 2023.
- [15] P. Di Barba, M.E. Mognaschi, A.M. Cavazzini, M. Ciofani, F. Dughiero, M. Forzan, M. Lazzarin, A. Marconi, D. Lowther, J. Sykulski. A Numerical Twin Model for the Coupled Field Analysis of TEAM Workshop Problem 36. In *IEEE Transactions on Magnetics*, 7000904, 59(5), 2023.
- [16] K. Derouiche, M. Daoud, K. Traidi, F. Chinesta. Realtime prediction by data-driven models applied to induction heating process. In *Int. J. of Material Forming*, 15(48), 2022.
- [17] S. Garois, M. Daoud, F. Chinesta. Explaining hardness modeling with XAI of C45 steel spur-gear induction hardening. *Int. J. of Material Forming*, 16(57), 2023.
- [18] P. Di Barba, F. Dughiero, M. Forzan, M.E. Mognaschi, E. Sieni. New solutions to a multi-objective benchmark problem of induction heating: an application of computational biogeography and evolutionary algorithms. In *Archives of Electrical Engineering*, pp. 139-149, 67(1), 2018.
- [19] D. Ha, A. Dai, Q.V. Le. HyperNetworks. *arXiv:1609.09106*, 2016.
- [20] F.A. Belbute-Peres, F. Sha, Y. Chen. HyperPINN: Learning parameterized differential equations with physics-informed hypernetworks. *arXiv:2111.01008v1*, 2021.
- [21] M. Baldan, P. Di Barba, D.A. Lowther. Physics-Informed Neural Networks for Inverse Electromagnetic Problems. In *IEEE Transactions on Magnetics*, pp. 1-5, 59(5), 2023.
- [22] P. Virtanen et. al. SciPy 1.0: Fundamental Algorithms for Scientific Computing in Python. In *Nature Methods*, pp. 261-272, 17, 2020.
- [23] F. Zhuang et al. A Comprehensive Survey on Transfer Learning. In *Proceedings of the IEEE*, pp. 43-76, 109(1), 2021.
- [24] Ansys Apdl, [www.ansys.com](http://www.ansys.com), Accessed: 2024-07-02